

Secular Bar-Mode Evolution and Gravitational Waves From Neutron Stars

Dong Lai

*Center for Radiophysics and Space Research, Department of Astronomy
Cornell University, Ithaca, NY 14853*

Abstract. The secular instability and nonlinear evolution of the $m = 2$ f-mode (bar-mode) driven by gravitational radiation reaction in a rapidly rotating, newly formed neutron star are reviewed. There are two types of rotating bars which generate quite different gravitational waveforms: those with large internal rotation relative to the bar figure (Dedekind-like bars) have GW frequency sweeping downward during the evolution, and those with small internal rotation (Jacobi-like) have GW frequency sweeping upward. Various sources of viscosity (which affects the instability) in hot nuclear matter are reexamined, and the possible effect of star-disk coupling on the bar-mode instability is also discussed.

I INTRODUCTION

Nonaxisymmetric instabilities can develop in rapidly rotating fluid bodies when the ratio $\beta \equiv T/|W|$ of the rotational energy T to the gravitational potential energy W is sufficiently large (e.g., Chandrasekhar 1969). In particular, the $l = m = 2$ f-mode (Kelvin mode), or bar-mode, becomes dynamically unstable when $\beta > \beta_{\text{dyn}} \simeq 0.27$. This β_{dyn} , originally derived for incompressible Maclaurin spheroid, is relatively insensitive to the equation of state and differential rotation (Pickett et al. 1996; Toman et al. 1998), although it tends to be reduced by general relativity (Shibata et al. 2000). The consequence of the dynamical bar-mode instability has been extensively studied using numerical simulations: the mode grows to nonlinear amplitude by shedding mass and angular momentum from the ends of the bar in the form of two-armed spiral pattern, and the central star assumes a bar shape that lasts many rotation periods (e.g., Tohline et al. 1985; New et al. 2000; Brown 2000; Shibata et al. 2000). It is important to note, however, that these simulations start out with a stationary, dynamically unstable star and such an initial condition may not be realized in an actual core collapse (e.g., Rampp, Müller and Ruffert 1998).

However, it is very likely that in a rotating core collapse (or neutron star binary merger), after the messy dynamics is completed, the newly formed NS settles down into a dynamically stable configuration, with $\beta < 0.27$, and yet still suffers further

secular, rotational instability. “Secularly unstable” means the instability is slow, and is driven by gravitational radiation reaction. In this paper, we will focus this secular instability and the possible gravitational wave signals from newly formed neutron stars in the first seconds/minutes of their lives.

II CFS INSTABILITY: F-, G- AND R-MODES

The gravitational radiation driven instability, or Chandrasekhar-Friedman-Schutz (CFS) instability (see e.g., Friedman 1998 for a review), arises for the following simple reason: Suppose in the rotating frame of the star we set up a perturbation (mode) (with frequency ω_r as in $e^{im\phi+i\omega_r t}$) which travels opposite to the rotation. In the inertial frame, the perturbation will be dragged backward by the rotation, and the mode frequency becomes $\omega_i = \omega_r - m\Omega_s$. If the spin Ω_s is sufficiently large, the perturbation will be prograde in the inertial frame. Since the mode has negative angular momentum (because the perturbed fluid does not rotate as fast as it did without the perturbation), as the mode radiates positive J through gravitational radiation, the mode’s angular momentum will be more negative; that means the mode is unstable.

The CFS instability mechanism can be applied to different modes of NSs:

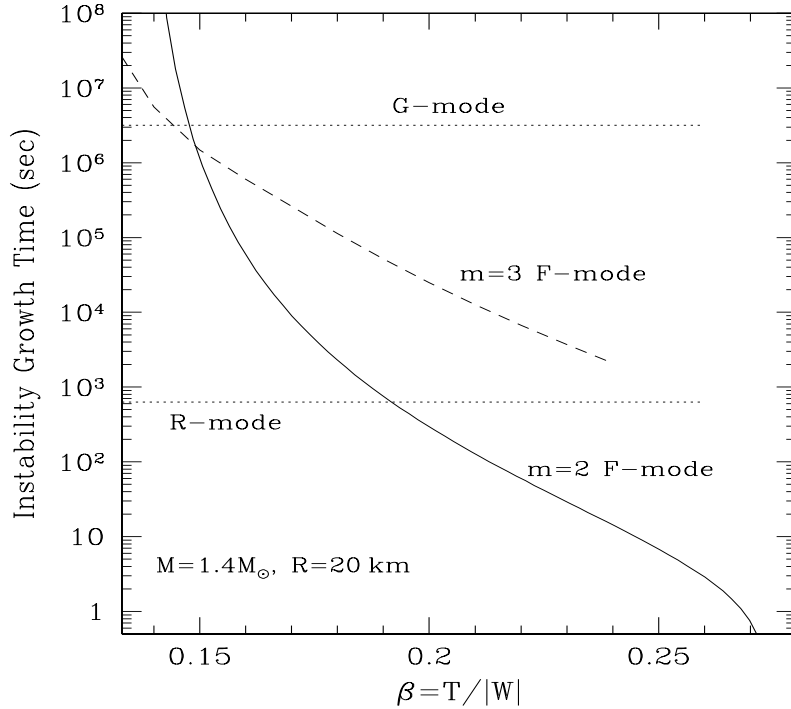


FIGURE 1. Growth times of gravitational radiation driven CFS instability for different modes in a neutron star as a function of β .

1. F-modes: The f-modes are fundamental acoustic waves, corresponding to a global distortion of the star. For the $m = 2$ mode (bar-mode), the instability occurs when $\beta > \beta_{\text{sec}} = 0.14$ — This critical β_{sec} is only slightly affected by equation of state, and is somewhat reduced (to as small as 0.1) by strong differential rotation (Imamura et al. 1995) and by general relativity (Stergioulas & Friedman 1998).

2. R-modes: In the last few years it was realized that the so-called r-modes are always secularly unstable (for stars consisting of inviscid fluid) (Andersson 1998) and the growth time of the mode through current quadrupole gravitational radiation can be interestingly short (Lindblom et al. 1998). A lot of works are currently being done on r-modes (see <http://online.itp.ucsb.edu/online/neustars00/si-rmode-sched.html> for a recent meeting devoted to r-modes), but they are beyond the scope of this paper (see Ushomirsky’s paper in this proceedings).

3. G-modes: G-modes are also unstable when Ω_s is (approximately) greater than the mode frequency (of nonrotating stars), which typically is ~ 100 Hz, or $0.1\Omega_{\text{max}}$. However, the growth time (despite the finite quadrupole moment) is quite long, and thus not interesting (Lai 1999).

Figure 1 shows a comparison of the CFS instability growth times for different modes in a $M = 1.4M_{\odot}$, $R_0 = 20$ km neutron star. We see that for sufficiently large β , the $m = 2$ f-mode (the bar-mode) is the most unstable mode, with the shortest growth time (of order seconds to minutes). So the bar-mode instability is most robust if a neutron star is formed with β in the range of 0.2 to 0.27 — numerical simulations indicate that this is indeed possible (Zwerger & Müller 1997; Rampp et al. 1998; see contributions by New and Brown). In the remainder of the paper we will be concerned with the bar-mode only.

The growth time shown in Fig. 1 is due to gravitational radiation only. There are several complications that can affect the net growth time. We will discuss two of them in the next two sections. Other issues, including the effect of magnetic field, can be found in Ho & Lai (2000).

III VISCOSITY IN PROTO-NEUTRON STARS

The first complication concerns the viscous dissipation, which tends to suppress the GR driven instability. For a proto-NS with $T \gtrsim 1$ MeV, the shear (kinematic) viscosity due to neutron-neutron scattering, $\nu = \eta/\rho \simeq 14 \rho_{15}^{5/4} T_{\text{MeV}}^{-2} \text{ cm}^2 \text{ s}^{-1}$ (Flowers & Itoh 1976), is negligible (since $t_{\text{visc}} \sim R^2/\nu$ is much greater than the growth time of the mode, t_{GR}). The shear viscosity due to neutrino-nucleon scattering is $\eta = n_{\nu} p_{\nu} l_{\nu}/5$ (Goodwin & Pethick 1982), where n_{ν} , p_{ν} , l_{ν} are the neutrino number density, momentum and scattering mean free path. Thus

$$\nu = \frac{\eta}{\rho} \sim c l_{\nu} \left(\frac{E_{\nu} n_{\nu}}{\rho c^2} \right) \sim 3 \times 10^6 \rho_{15}^{-4/3} T_{\text{MeV}} \text{ cm}^2 \text{ s}^{-1}, \quad (1)$$

where we have used $l_{\nu} \simeq 2000(E_{\nu}/30 \text{ MeV})^{-3} \text{ cm}$. Contrary to some earlier claims (e.g., Lindblom & Detweiler 1979), the neutrino shear viscosity is also negligible.

The most relevant viscosity in a proto-NS is the bulk viscosity. This arises from the fact that in an oscillation which involves compression, the matter will be temporarily out of chemical equilibrium (in this case, β -equilibrium between n,p,e) and it will try to relax back to the equilibrium by the weak processes

$$e + p \rightarrow n + \nu_e, \quad n \rightarrow p + e + \bar{\nu}_e, \quad (\text{URCA}) \quad (2)$$

or

$$e + p + N \rightarrow n + N + \nu_e, \quad n + N \rightarrow p + N + e + \bar{\nu}_e, \quad (\text{Modified URCA}) \quad (3)$$

and therefore emitting neutrinos; this neutrino emission serves as damping of the oscillation.

The standard bulk viscosity widely used in the last decade has been the one derived by Sawyer (1989) (correcting a factor of 100 typographic error)

$$\zeta = 1.5 \times 10^{32} \rho_{15}^2 T_{\text{MeV}}^6 \omega^{-2} \text{ g}/(\text{cm s}), \quad (\text{Modified URCA}) \quad (4)$$

where T_{MeV} is the temperature in MeV, $\rho = 10^{15} \rho_{15} \text{ g}/\text{cm}^3$ is the density, and ω is the mode (angular) frequency in s^{-1} . This is quite large, with the corresponding damping time $R^2 \rho / \zeta \sim 10 T_{\text{MeV}}^{-6} \text{ s}$ for $\omega \sim 10^3 \text{ s}^{-1}$. Thus one may conclude that the bar-mode instability is suppressed for $T_{\text{MeV}} \gtrsim 1$ (see Iperser & Lindblom 1991 for more detailed computations). Similarly, if direct URCA process operates, equation (4) should be replaced by

$$\zeta \simeq 1.5 \times 10^{36} \rho_{15}^2 T_{\text{MeV}}^4 \omega^{-2} \text{ g}/(\text{cm s}) \quad (\text{URCA}) \quad (5)$$

where we have used the free npe gas relation $n_e/n_0 = 0.0765 \rho_{15}^2$ ($n_0 = 0.16 \text{ fm}^{-3}$) to evaluate the equilibrium electron density (this is not consistent since in a free npe gas URCA processes are suppressed; but it is adequate for estimate). Equation (5) is valid for $\omega \gg 118 x^{-2/3} T_{\text{MeV}}^4 \text{ s}^{-1}$ (where the electron fraction $x = n_e/n = 0.02 \rho_{15}$).

However, one should be careful when using eqs. (4)-(5) at high temperatures. In fact, when T becomes sufficiently large, the bulk viscosity must go down. The reason is that as T increases, the timescale to relax back to β -equilibrium becomes shorter than the oscillation period. So the matter will stay very close to β -equilibrium during the oscillation and there is very little extra neutrino emission associated with the oscillation. Another effect that needs to be included at high temperatures is neutrino absorption (such as $\nu_e + n \rightarrow e + p$) which also helps to speed up relaxation to β -equilibrium.

We now outline the derivation of the neutrino bulk viscosity in the regime where matter is opaque to neutrinos (see Sawyer 1980; Lai 2001). Consider the emission and absorption of ν_e 's. The ν_e distribution function f satisfies the Boltzmann equation

$$\frac{\partial f}{\partial t} = j - \kappa f, \quad (6)$$

where j is the emissivity, and $\kappa = j \left(1 + e^{\frac{E-\delta\mu}{T}}\right)$ is the absorption cross section per unit volume (corrected for the effect of stimulated absorption), $\delta\mu \equiv \mu_e + \mu_p - \mu_n$. In equilibrium ($\delta\mu = 0$; we assume $\mu_\nu = 0$), we have $f = f_0 = f_{eq} = \left(1 + e^{\frac{E}{T}}\right)^{-1}$ and $j_0 = \kappa_0 f_0$. In a perturbation with $\delta f \propto e^{i\omega t}$, we find

$$(i\omega + \kappa_0)\delta f = \frac{e^{E/T}}{(1 + e^{E/T})^2} \left(\frac{\delta\mu}{T}\right) \kappa_0. \quad (7)$$

Similar consideration for $\bar{\nu}_e$ gives $(i\omega + \bar{\kappa}_0)\delta \bar{f} = -e^{E/T}(1 + e^{E/T})^{-2} (\delta\mu/T) \bar{\kappa}_0$, where we have used $\bar{j}_0 = j_0$ and $\bar{\kappa}_0 = \kappa_0$. The variation of electron fraction $x = n_e/n$ is

$$\delta x = -\frac{1}{n} \int \frac{d^3p}{(2\pi)^3} (\delta f - \delta \bar{f}) \simeq -\frac{\delta\mu}{(i\omega + \kappa_0)n} \lambda_{\text{eff}}, \quad (8)$$

where $\lambda_{\text{eff}} = T^2 \kappa_0/6$. Since the matter is degenerate to a good approximation, $\delta\mu$ depends only on ρ, x . Thus

$$\delta x = -\frac{\lambda_{\text{eff}}/\rho}{i\omega + \kappa_{\text{eff}}} \left(\frac{\partial \delta\mu}{\partial n}\right)_x \delta\rho, \quad (9)$$

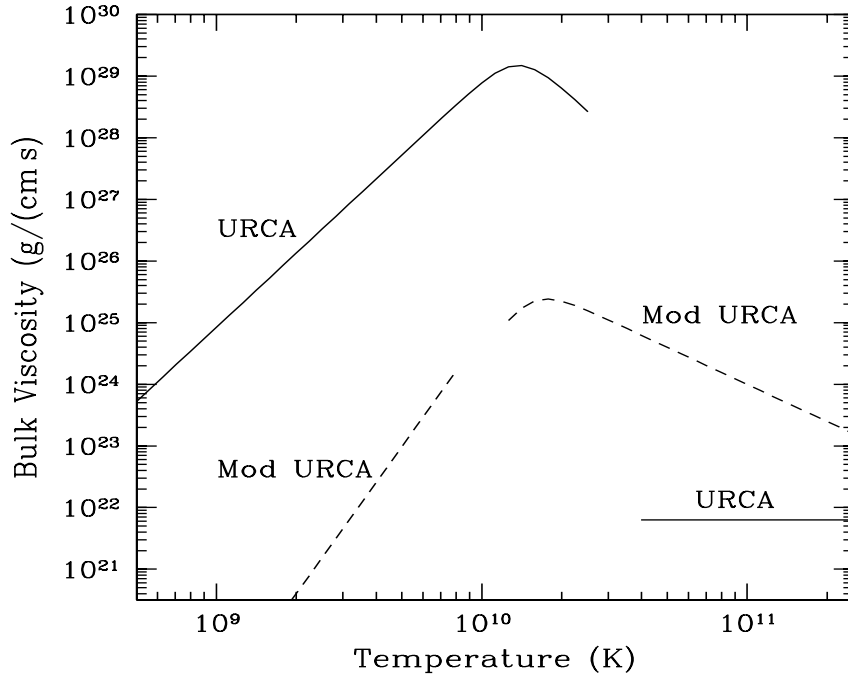


FIGURE 2. Bulk viscosity ζ as a function of temperature. The lower temperature segments correspond to (neutrino) optically thin regime, and the high temperature segments to the opaque regime. The density is $\rho_{15} = 1$, and the mode frequency $\omega/(2\pi) = 10^3$ Hz.

where $\kappa_{\text{eff}} = \kappa_0 + (\lambda_{\text{eff}}/n) (\partial\delta\mu/\delta x)_n$. The energy dissipation rate per unit volume (averaged over oscillation period) can be calculated by

$$\langle \dot{E} \rangle = \frac{1}{\rho} \left\langle \delta P \frac{d\delta\rho}{dt} \right\rangle = \frac{1}{2\rho} (\delta\rho)^2 \text{Re} \left[(-i\omega) \frac{\delta P}{\delta\rho} \right] \equiv \frac{1}{2} \zeta \omega^2 \left(\frac{\delta\rho}{\rho} \right)^2. \quad (10)$$

Using eq. (9) we then find the bulk viscosity

$$\zeta = \frac{\lambda_{\text{eff}}}{\omega^2 + \kappa_{\text{eff}}^2} \left(\frac{\partial\delta\mu}{\partial n} \right)_x \left(\frac{\partial P}{\partial x} \right)_\rho = \frac{\lambda_{\text{eff}}}{\omega^2 + \kappa_{\text{eff}}^2} \left(\frac{\mu_n}{3} \right)^2, \quad (11)$$

where the second equality applies for free npe gas ($\mu_n = 140 \rho_{15}^{2/3}$ MeV is the neutron Fermi energy), for which $(\partial\delta\mu/\partial x)_n = 3(n/n_e)\mu_n$ and thus $\kappa_{\text{eff}} \simeq \kappa_0$.

For modified URCA process, we have

$$\kappa_0 = 1.034 \times 10^3 \rho_{15}^{2/3} T_{\text{MeV}}^4 \text{ s}^{-1}, \quad (12)$$

$$\zeta = 7.9 \times 10^{31} \rho_{15}^2 T_{\text{MeV}}^6 (\omega^2 + \kappa_0^2)^{-1} \text{ g}/(\text{cm s}). \quad (\text{Modified URCA}) \quad (13)$$

If direct URCA process operates (which requires sufficiently large x , a condition necessarily satisfied at early times of the proto-neutron star), we have

$$\kappa_0 = 1.13 \times 10^7 \rho_{15}^{2/3} T_{\text{MeV}}^2 \text{ s}^{-1}, \quad (14)$$

$$\zeta = 6.7 \times 10^{21} \rho_{15}^{2/3} \text{ g}/(\text{cm s}), \quad (\text{URCA}) \quad (15)$$

where the ζ expression is evaluated in the $\kappa_0 \gg \omega$ limit. We see from Fig. 2 that for $T \gtrsim$ MeV, the viscosity is less than 10^{25} g/(cm s) (depending on whether URCA or modified URCA processes operates), and thus the bulk viscosity cannot suppress the CFS instability of the bar-mode (see Lai 2001 for more details).

IV EFFECT OF STAR–DISK COUPLING

A newly formed rotating neutron star is often surrounded by a disk. As the bar grows in the NS, it will excite density waves in the disk, and therefore transfers angular momentum to the disk or from the disk. This will either enhance or suppress the bar-mode instability — this is simply another form of CFS instability.

The angular momentum transfer is mainly through the so-called Lindblad resonances, where $2(\Omega_p - \Omega_k) = \pm\Omega_k$ ($\Omega_p = \omega_i/2$ is the pattern rotation of the bar and Ω_k is the rotation of the disk, assumed to be Keplerian). The torques can be calculated using the formalism of Goldreich & Tremaine (1979). At the inner Lindblad resonance (ILR), $\Omega_k = 2\Omega_p$, the driving rate of the bar-mode due to star–disk coupling is (Lai 2001)

$$\gamma_{\text{ILR}} \simeq -\frac{6\pi^2}{5} \frac{\Omega_p^2}{(\Omega_s - 2\Omega_p)} \frac{\Sigma(r_{\text{ILR}})}{(M/R_e^2)}, \quad (16)$$

where the negative sign in the front implies that the torque tends to damp the mode, Ω_s is the rotation rate of the star, R_e is the equatorial radius, and $\Sigma(r_{\text{ILR}})$ is the surface density of the disk evaluated at ILR. Similarly, at the outer Lindblad resonance (OLR), we have

$$\gamma_{\text{OLR}} \simeq \frac{98\pi^2}{45} \frac{\Omega_p^2}{(\Omega_s - 2\Omega_p)} \frac{\Sigma(r_{\text{OLR}})}{(M/R_e^2)}, \quad (17)$$

where the positive front sign means that the torque drives the CFS instability. Clearly, the net effect of star-disk coupling on the mode depends on the relative importance of ILR and OLR. Compared with driving rate of the mode due to gravitational radiation, we find that star-disk coupling is important when $\Sigma \gtrsim 10^{-6} M/R_e^2$. So even a small amount of material outside the proto-NS may potentially affect the CFS instability of the bar-mode.

V NONLINEAR EVOLUTION OF BAR-MODE AND GRAVITATIONAL WAVEFORMS

In general, to determine the nonlinear evolution of the bar-mode requires 3d hydrodynamical simulations including gravitational radiation reaction, and one needs to follow the system for a time much longer than the dynamical time of the star. This possesses a significant technical challenge (see recent attempt by Lindblom et al. 2000 on the r-mode evolution where an approximate ansatz for the radiation reaction is adopted).

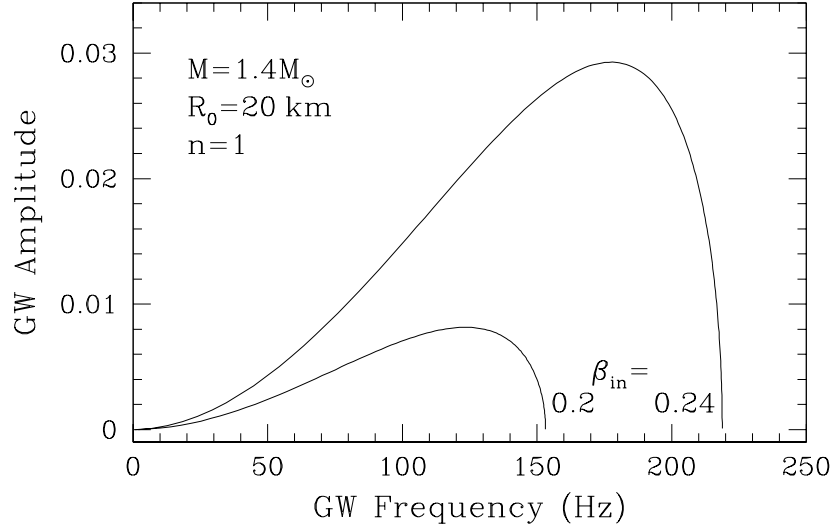


FIGURE 3. The amplitudes of the GWs emitted by a secularly unstable NS, evolving from a Maclaurin spheroid toward a Dedekind ellipsoid. The two curves correspond to initial $\beta = 0.24$ and 0.2 respectively ($n = 1$ is the polytropic index). The GW frequency sweeps downward.

A Dedekind-like Bar

One of the advantages of the $m = 2$ f-mode (as opposed the higher m f-modes and or r-modes) is that under certain idealized condition, namely for incompressible fluid, there exists an exact solution for the nonlinear development of the bar-mode instability driven by gravitational radiation (Miller 1974; see Lai & Shapiro 1995 and references therein; the latter also includes an approximate, compressible generalization).

The evolutionary sequence is as follows: We start with an axisymmetric Maclaurin spheroid with $\beta > 0.14$ (secularly unstable). The bar grows and has a pattern angular frequency Ω_p (which is related to the mode frequency in the inertial frame by $\Omega_p = \omega_i/2$). Relative to the bar, there is also an internal rotation Ω_{in} which is larger than Ω_p . The important point to note is that although the mean rotation of the star $\Omega_s \simeq \Omega_p + \Omega_{in}$ is near breakup, Ω_p can be much smaller (in fact, at the bifurcation point $\beta = 0.14$, we have $\Omega_p = 0$). As the amplitude of the bar continues to grow, the bar also gradually slows down. Eventually we reach a configuration with zero pattern speed. This is the Dedekind ellipsoid, basically stationary “football” with a fixed figure in space but with a lot internal rotation Ω_{in} .

The gravitational wave (GW) emitted during such a quasi-equilibrium secular evolution is quite interesting. Figure 3 shows the GW amplitude as a function of GW frequency. The GW is quasi-periodic. Initially, we have an axisymmetric star, so $h = 0$. Then the GW amplitude increases as the bar grows. In the meantime, the bar slows down and the GW frequency ($= 2\Omega_p$) decreases. So eventually h decreases. Thus we have a non-monotonic GW amplitude evolution, with the GW frequency sweeps downward from a few hundred Hertz toward zero. The timescale

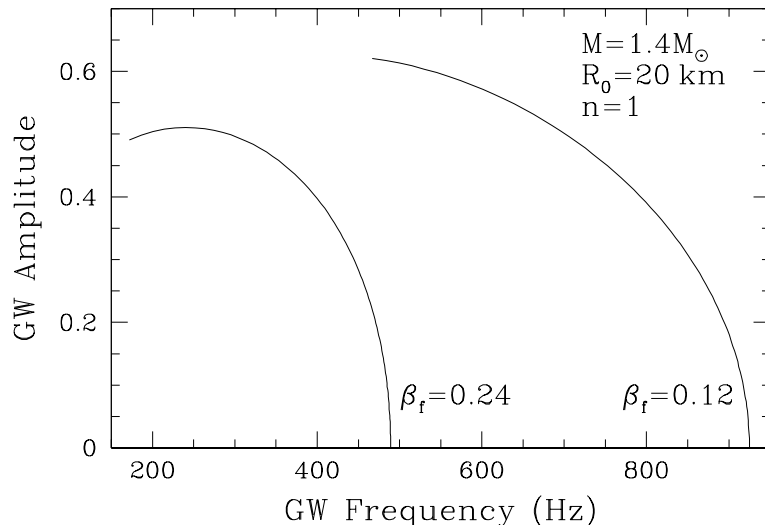


FIGURE 4. The amplitudes of the GWs emitted by Jacobi-like bars. The two curves correspond to final $\beta = 0.24$ and 0.12 respectively. The GW frequency sweeps upward.

of the evolution is of order seconds to minutes, and the characteristic number of cycles of GWs is of order 10^4 .

So far we have assumed the star begins its evolution from an axisymmetric state. Recent numerical simulations (e.g., New et al. 2000,; Brown 2000; Shibata et al. 2000), however, indicate that at the end of the dynamical evolution, the star may be already elongated rather than axisymmetric. So one can ask about the long-term evolution of the bar and the emitted GWs. Here the ellipsoid model can also provide qualitative answers. There are two possibilities (see Lai & Shapiro 1995 for details): (1) If the bar has $\Omega_{in} > \Omega_p$, namely if the bar is *Dedekind-like*, then the evolution and waveform discussed above should also apply except that we need to cut off the initial growth phase of the bar. (2) Another possibility occurs when $\Omega_p > \Omega_{in}$, which we discuss in the next subsection.

B Jacobi-like Bar

If the bar has internal rotation (relative to the bar figure) less than the pattern rotation, i.e., $\Omega_{in} < \Omega_p$, the bar is called *Jacobi-like*, and the evolution is quite different. In this case, gravitational radiation reaction tends to decrease the amplitude of the bar, making the star less elongated. In the meantime, Ω_p increases because, even though J decreases, the moment of inertia decreases faster. So the GW frequency increases and eventually the star becomes axisymmetric. Here again we have a quasi-periodic GW signal (see Fig. 4), except that the frequency sweeps upwards. The timescale for the evolution is of order a second, and the number of cycles is of order a few hundred.

Note that at the end of the Jacobi-like evolution, the axisymmetric star may still be secularly unstable. If so the star will continue to evolve in the way described in Sec. V.A.

C Characteristic GW Amplitude

To recapitulate, there are two types of rotating bars, and their evolution and emitted GWs are qualitatively different: (1) A Dedekind-like bar has large internal rotation, and the resulting waveform sweeps downward in frequency; (2) A Jacobi-like bar has relatively small internal rotation, and the GW frequency sweeps upwards. Figure 5 shows the characteristic GW amplitudes for the two types of bars compared with the sensitivity curves (h_{rms}) of LIGO I,II and III. The characteristic GW amplitude is given by (Lai & Shapiro 1995)

$$h_c = h \left| \frac{dN}{d \ln f} \right|^{1/2} = \frac{M}{D} \left(\frac{R_0}{M} \right)^{1/4} \left(\frac{5}{2\pi} \left| \frac{d\bar{E}}{d\bar{\Omega}_p} \right| \right)^{1/2}, \quad (18)$$

where D is the distance, $|dN/d \ln f| = |f^2/\dot{f}|$ is the number of cycles of GW spent near frequency f , $E = \bar{E}(M^2/R_0)$ is the energy of the star, and $\Omega_p = \bar{\Omega}_p(M/R_0^3)^{1/2}$

is its angular pattern speed. For a broad band detector such as LIGO, the best signal-to-noise ratio will be obtained by matched filtering of the data, with $S/N \simeq h_c/h_{\text{rms}}$. Note that unlike coalescing compact binaries, the phase evolution of the GW from the evolving bars can not be determined with the accuracy needed for matched filtering, so such a high S/N may not be achieved in practice. A new fast chirp transform technique (Jenet & Prince 2000) is promising for detecting such signals.

The event rate of Type II SNe at distance of 30 Mpc is about 100 per year. So even if a small fraction of the NSs are formed rotating rapidly, the GW signals discussed here are promising for LIGO. Of course, it should be emphasized that the waveforms discussed in this section are based on the exact solution for the idealized situation (incompressible fluid). Whether this idealized solution has any resemblance to reality remains to be seen by future studies.

VI PARAMETRIZED WAVEFORMS

Finally we give fitting formulae for the gravitational waveforms generated by a rapidly rotating NS as it evolves from an initial axisymmetric configuration toward a triaxial ellipsoid (Maclaurin spheroid \Rightarrow Dedekind ellipsoid) as discussed in

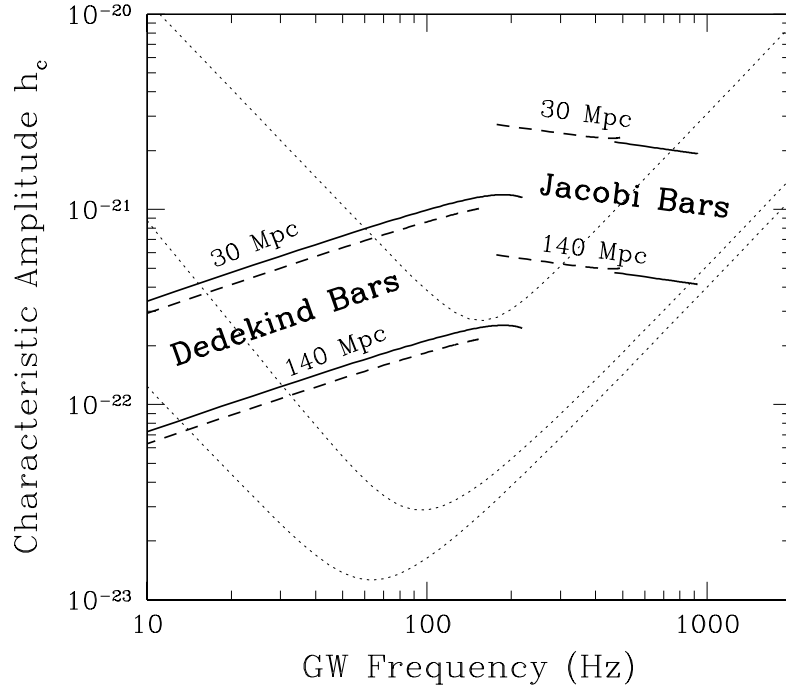


FIGURE 5. Comparison between the characteristic GW amplitudes h_c emitted during the secular evolution of a nonaxisymmetric neutron star and the rms noise h_{rms} of LIGO I,II and III. The solid and dashed lines correspond to the two different cases in Fig. 3 and Fig. 4.

Sec. V.A. We use units such that $G = c = 1$.

The waveform (including the polarization) is given by eq. (3.6) of Lai & Shapiro (1995) (hereafter LS). Since the waveform is quasi-periodic, we will give fitting formulae for the wave amplitude h (Eq. [3.7] of LS) and the quantity $(dN/d \ln f)$ (eq. [3.8] of LS; related to the frequency sweeping rate), from which the waveform $h_+(t)$ and $h_\times(t)$ can be easily generated in a straightforward manner.

1. Wave Amplitude: The waveform is parametrized by three numbers: f_{max} is the maximum wave frequency in Hertz, $M_{1.4} = M/(1.4M_\odot)$ is the NS mass in units of $1.4M_\odot$, $R_{10} = R/(10 \text{ km})$ is the NS radius in units of 10 km. (Of course, the distance D enters the expression trivially.) It is convenient to express the dependence of h on t through f (the wave frequency), with $f(t)$ to be determined later. A good fitting formula is

$$h[f(t); f_{max}, M, R] = \frac{M^2}{DR} A \left(\frac{f}{f_{max}} \right)^{2.1} \left(1 - \frac{f}{f_{max}} \right)^{0.5}, \quad (19)$$

where

$$A = \begin{cases} (\bar{f}_{max}/1756)^{2.7}, & \text{for } \bar{f}_{max} \leq 400 \text{ Hz;} \\ (\bar{f}_{max}/1525)^3, & \text{for } \bar{f}_{max} \geq 400 \text{ Hz;} \end{cases} \quad \text{with } \bar{f}_{max} \equiv f_{max} R_{10}^{3/2} M_{1.4}^{-1/2}. \quad (20)$$

Note that if we want real numbers, we have

$$\frac{M^2}{DR} = 4.619 \times 10^{-22} M_{1.4}^2 R_{10}^{-1} \left(\frac{30 \text{ Mpc}}{D} \right). \quad (21)$$

2. Number of GW cycles: The fitting formula is

$$\left| \frac{dN}{d \ln f} \right| = \left(\frac{R}{M} \right)^{5/2} \frac{0.016^2 (R_{10}^{3/2} M_{1.4}^{-1/2} f / 1 \text{ Hz})}{A^2 (f/f_{max})^{4.2} [1 - (f/f_{max})]}. \quad (22)$$

Notes to the fitting formulae:

Note (i): Using the above equations, we obtain the characteristic amplitude:

$$\begin{aligned} h_c = h \left| \frac{dN}{d \ln f} \right|^{1/2} &= 0.016 \frac{M^{3/4} R^{1/4}}{D} \left(\frac{R_{10}^{3/2} M_{1.4}^{-1/2} f}{1 \text{ Hz}} \right)^{1/2} \\ &= 5.3 \times 10^{-23} \left(\frac{30 \text{ Mpc}}{D} \right) M_{1.4}^{3/4} R_{10}^{1/4} \left(\frac{R_{10}^{3/2} M_{1.4}^{-1/2} f}{1 \text{ Hz}} \right)^{1/2}, \end{aligned} \quad (23)$$

which agrees with Eq. (3.12) of LS to within 10% [Note that in Eq. (3.12) of LS, the factor $f^{1/2}$ should be replaced by $(R_{10}^{3/2} M_{1.4}^{-1/2} f)^{1/2}$, similar to the above expression.]

Note (ii): The accuracy of these fitting formulae (as compared to the numerical results shown in LS) is typically within 10%. When f is very close to f_{max} , the error in the fitting can be as large as 30%.

Note (iii): The frequency evolution $f(t)$ is obtained by integrating the equation $f^2/\dot{f} = -|dN/d\ln f|$ (note that the frequency sweeps from f_{max} to zero). For example, we can choose $t = 0$ at $f = 0.9f_{max}$. (Note that one should not choose $t = 0$ at $f = f_{max}$ as the time would diverge — the actual evolution near f_{max} depends on the initial perturbations). Once $f(t)$ is obtained, the waveform can be calculated as (cf. Eq. [3.6] of LS):

$$h_+ = h[f(t); f_{max}, M, R] \cos \Phi(t) \frac{1 + \cos^2 \theta}{2}, \quad (24)$$

$$h_\times = h[f(t); f_{max}, M, R] \sin \Phi(t) \cos \theta, \quad (25)$$

where θ is the angle between the rotation axis of the star and the line of sight from the earth, and $\Phi(t) = 2\pi \int f(t)dt$ is the phase of the gravitational wave.

Note (iv): f_{max} typically ranges from 100 Hz to 1000 Hz (see Fig. 5 of LS); $M_{1.4}$ and R_{10} are of order unity for realistic neutron stars.

REFERENCES

1. Andersson, N. 1998, ApJ, 502, 708
2. Brown, J.D. 2000, gr-qc/0004002.
3. Chandrasekhar, S. 1969, “Ellipsoidal Figures of Equilibrium” (Yale Univ. Press).
4. Flowers, E., & Itoh, N. 1976, ApJ, 206, 218.
5. Friedman, J.L. 1998, in “Black Holes and Relativistic Stars”, ed. R.M. Wald (Univ. Chicago Press).
6. Goldreich, P., and Tremaine, S. 1979, ApJ, 233, 857.
7. Goodwin, and Pethick, C.J. 1982, ApJ, 253, 816.
8. Ho, W.C.G., and Lai, D. 2000, ApJ, 543, 386.
9. Imamura, J., et al. 1995, ApJ, 444, 363.
10. Jenet, F.A., and Prince, T.A. 2000, gr-qc/0012029.
11. Lai, D. 1999, MNRAS, 307, 1001.
12. Lai, D., and Shapiro, S.L. 1995, ApJ, 442, 259.
13. Lindblom, L., and Detweiler, S. 1979, ApJ, 232, L101.
14. Lindblom, L., Owen, B.J., & Morsink, S.M. 1998, Phys. Rev. Lett., 80, 4843.
15. Lindblom, L., Tohline, J.E., and Vallisneri, M. 2000, astro-ph/0010653.
16. Miller, B.D. 1974, ApJ, 187, 609.
17. New, K.C.B., Centrella, J.M., and Tohline, J.E. 2000, Phys. Rev. D62, 064019.
18. Pickett, B.K., Durisen, R.H., and Davis, G.A. 1996, ApJ, 458, 714.
19. Rampp, M., Müller, E., and Ruffert, M. 1998, A&A, 332, 969.
20. Saijo, M., Shibata, M., Baumgarte, T.W., and Shapiro, S.L. 2000, astro-ph/0010201
21. Sawyer, R.F. 1989, Phys. Rev. D, 39, 3804.
22. Shibata, M., Baumgarte, T.W., and Shapiro, S.L. 2000, astro-ph/0005378
23. Stergioulas, N., and Friedman, J.L. 1998, ApJ, 492, 301.
24. Tohline, J., Durisen, R., and McCollough, M. 1985, ApJ, 298, 220.
25. Toman, J., Imamura, J.N., Prickett, B.J., and Durisen, R.H. 1998, ApJ, 497, 370.
26. Zwerger, T., & Müller, E. 1997, A&A, 320, 209.